Cyclodextrin Cavity Size Effect on the Complexation and Rotational Dynamics of the Laser Dye 2,5-Diphenyl-1,3,4-oxadiazole: From Singly Occupied Complexes to Their Nanotubular Self-Assemblies

George Pistolis* and Ioanna Balomenou

NCSR 'Demokritos' Institute of Physical Chemistry, 153 10 Athens, Greece

Received: March 31, 2006; In Final Form: May 17, 2006

The general complexation scheme as well as the dynamic features of the supramolecular structures resulting from the interaction of the laser dye 2,5-diphenyl-1,3,4-oxadiazole (PPD) with the naturally occurring α-, β-, and γ-cyclodextrins in water are studied by means of fluorescence spectroscopy, both steady-state (SS) and time-resolved (TR). PPD interacts weakly, from a thermodynamic point of view, with α-cyclodextrin (α-CD), forming 1:1 complexes with an association constant of $K_{11} = 85 \pm 4\ M^{-1}$. However, the local motion of the substrate (PPD) with respect to the ligand (CD) in the complexed form is hindered; namely, dynamically, they are strongly coupled and only a *global* tumbling motion, $\tau^{gl}_{r(11)} = 370 \pm 30$ ps, of the whole adduct is observed. The next homologue β-CD also forms 1:1 entities with PPD, but although the binding strength of reactants ($K_{11} = 682 \pm 60\ M^{-1}$) is almost an order of magnitude greater than the former case with the α-CD, these are dynamically weakly coupled. In fact, two independent motions are detected: one is that of the whole nanostructure motion (1:1, PPD/β-CD) with a *global* rotational relaxation time of $\tau^{gl}_{r(11)} = 480 \pm 30$ ps, and the other is an internal librational motion of the dye inside the host cavity with an average angular displacement of $\theta \sim 27°$. Finally, the interaction of PPD with the wider and more flexible cavity of the γ-CD "triggers" a self-associative scheme of the initially formed supramolecular building blocks, namely, singly occupied complexes, leading to the formation of nanotubular superstructures. It is found that these linear arrays are constituted from more than 17 γ-CD units which are held together with the aid of dimers of PPD. Interestingly, our results supported that two distinct dimeric forms of PPD play the role of the "shaft" between adjacent cyclodextrin units. The topology of the dimers in the interlinking space of γ-CD units is such that PPD molecules are held in suitable proximity, resulting, upon excitation, in the observation of dual excimer emission.

1. Introduction

The spontaneous self-assembly of organic *subunits* (*molecules*, *macromolecules*, and *supramolecules*) into well-defined architectures in the solid state or in solution is a topic of intense current research.[1,2] Moreover, self-assembly is a more practical strategy to organize matter on a larger scale than that of molecules synthesized bond by bond. These issues are important not only from a fundamental point of view but also for their potential multidisciplinary applications, spanning from biology[2] to supramolecular chemistry and nanoscience−nanotechnology. Most importantly, a renewed interest in supramolecular chemistry has yielded numerous supramolecular architectures of relevance to organic electronic devices,[3] switches,[4] sensors,[5] materials with a nonlinear optical response,[6] nanotubes,[7] molecular zeolites,[8] and so forth.

Cyclodextrins,[9] and in particular the so-called α, β, and γ homologues (Scheme 1), are among the most interesting and functional host materials. They have a rigid, well-defined ring structure and an ability to incorporate in their hydrophobic cavity various inorganic and organic molecules mainly via hydrophobic and van der Waals interactions. Inclusion complexes of 1:1 and/or 1:2 stoichiometry (guest/host) have been widely observed in aqueous solutions,[9] as a result of the combination of several parameters, as for example hydrophobicity, chirality, and most importantly the size/shape of the guest and the size of the cyclodextrin employed. Moreover, it has been found that the interaction of appropriate linear oligomeric or polymeric chains with some cyclodextrins can lead to supramolecular assemblies such as rotaxanes,[10] polyrotaxanes,[11] and threaded cyclodextrins[12] which do not involve any covalent bonding between the starting reactants.

Another strategy to produce supramolecular architectures includes the interaction of cyclodextrins with some small rodlike molecules. Although cyclodextrin molecules themselves do not interact with each other in aqueous solutions, in the presence of an appropriate rodlike guest, the initially formed supramolecular building blocks, namely, singly occupied complexes, are self-assembled to form complex architectures[13−16] which can be viewed as polypseudorotaxanes[12] often referred to as "supramolecular polymers".[13,14] In these superstructures, the rodlike guest plays the role of a "shaft" between adjacent cyclodextrins, whereas noncovalent interactions such as van der Waals, hydrophobic, and hydrogen bonding assist in the stabilization of the whole adduct. Specifically, it is found that some oxazole,[13] oxadiazole,[14] diphenylpolyene,[15] and coumarin[8] derivatives form oligomeric nanotube inclusion complexes mainly with γ-cyclodextrin. Therefore, a better understanding of the role of the different parameters involved in the self-organization of host/guest systems will provide new criteria in

* To whom correspondence should be addressed. E-mail: pistolis@chem.demokritos.gr. Fax: +30 210 6511766.

10.1021/jp062003p CCC: $33.50
Published on Web 08/01/2006

SCHEME 1: Cyclodextrins and 2,5-Diphenyl-1,3,4-oxadiazole (PPD)[a]

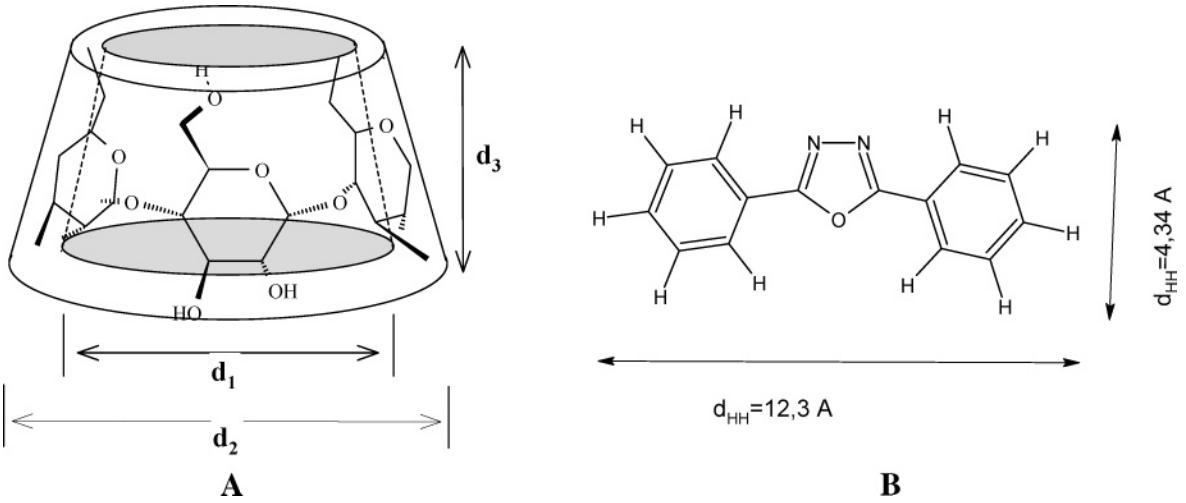

[a] Characteristics of CDs are given in ref 9d.

designing novel superstructures. Thus, starting from the procedures employed by us, where control on the average length of oligomeric nanotubes[16] constituted by inclusion complexes between α,ω-diphenylpolyenes and γ-cyclodextrin was obtained by varying the guest size, we intend now to further explore the crucial role of the cavity size effect on the possible formation of these superstructures.

More specifically, the objective of the present work was to comprehensively study how the systematic increase of the cyclodextrin cavity size affects not only the structure, geometry, and binding strength (wherever possible) of the resulting supramolecular adducts but also their dynamic features. We chose the laser dye 2,5-diphenyl-1,3,4-oxadiazole[17] (PPD) for two major reasons: one is that it possesses the simplest rodlike structure that forms the aforementioned assemblies, as previously reported mostly qualitatively,[14a] and the other is that it is a fluorescence probe with excellent photophysical properties, namely, high fluorescence quantum yield and suitable lifetime and anisotropy, ideal for signaling complex recognition events. It is worth noting that molecular and macromolecular recognition events can be signaled qualitatively and quantitatively with fluorescence sensors owing to the substantial alteration of the photophysical properties of the latter induced by environmental stimuli. These changes are observable even in very dilute solutions where other powerful techniques such as NMR are not applicable.[18] Considering that the aforementioned supramolecular polymers are usually characterized by an infinitely low solubility in water,[16] the potential of the fluorescence spectroscopy is the only useful characterization tool.

Of special interest, however, is the depolarization of the emission which can be caused by a number of phenomena including molecular motion/rotation and excitation energy transport phenomena.[18] Rotational diffusion(s) of fluorophores that are restricted in the environment of a host, that is, a cyclodextrin cavity, is one common cause of depolarization. These diffusive motions depend, in turn, upon the viscosity of the solvent and the size and shape of the rotating species. Thus, the average length and consequently the average molecular weight (MW) of the assembled nanostructure can be estimated with satisfactory accuracy. Extending these measurements into the time domain (time-resolved fluorescence anisotropy (TRFA) measurements), additional *unique* information relating not only to the *self-assembly route* but also to the *dynamics* of these processes can be obtained.

2. Experimental Section

Cyclodextrins (α-, β-, and γ-CDs) were purchased from Cyclolab. The 2,5-diphenyl-1,3,4-oxadiazole (PPD) was obtained from Aldrich. All chemicals were of the highest purity available and were used as received. Absorption spectra were recorded on a Perkin-Elmer Lambda-16 spectrophotometer, whereas for steady-state fluorescence anisotropy measurements we used the LS-50B Perkin-Elmer fluorometer. Fluorescence lifetimes (τ_f) were determined using the time-correlated single-photon counter FL900 of Edinburgh Instruments, which is capable of measuring lifetimes down to 80 ps. The determinations of fluorescence quantum yields (Φ) and steady-state anisotropies (r_{ss}) have been described elsewhere.[19] As the standard reference for quantum yield determinations, a very dilute solution of *p*-terphenyl in cyclohexane ($\Phi_s = 0.84$)[20] was used. The temperature was kept at 23 ± 0.2 °C for all measurements. All computer fits and simulations, except those of time-resolved analysis, were performed using the program "MicroMath Scientist for Windows", version 2.01, of MicroMath Inc.

Rotational reorientation times were measured using subnanosecond time-resolved fluorescence depolarization spectroscopy with a time-correlated single-photon counting technique. Time-resolved fluorescence anisotropy ($r(t)$) defined according to eq 1,

$$r(t) = \frac{D(t)}{S(t)} = \frac{GI_{VV}(t) - I_{VH}(t)}{GI_{VV}(t) + 2I_{VH}(t)} \qquad (1)$$

was measured using the time-correlated single-photon counter FL900 of Edinburgh Instruments. In eq 1, $D(t)$ and $S(t)$ are the so-called difference and sum functions, I_{VV} is the fluorescence intensity when the excitation and emission polarizers are parallel, I_{VH} is the fluorescence intensity for mutually perpendicular polarizers, and $G = I_{HH}(t)/I_{HV}(t)$ is a correction factor dependent on the emission wavelength. Time increments of 49 ps/ch were used to measure the decays of the caged dye in cyclodextrin cavities. These decays were convoluted with the instrument response function, which was measured by replacing the sample with a solution that scatters light. The instrument response function has a full width at half-maximum of 780 ps. Two different approaches were employed to fit the polarized decay traces, namely, the *spherical rotor anisotropy model*[18] and the *impulse reconvolution analysis*.[21]

2.1. Spherical Rotor Anisotropy Model. Simultaneous fits of both the parallel and crossed (perpendicular) decay components (subscripts p and x, respectively) were done using a nonlinear least-squares routine that uses the Marquardt algorithm. The fit produces an overall global minimum for both crossed and parallel decays in an attempt to find the best set of fit parameters. The fits produced are of the form

$$Y_x(t) = A_x + B_x[1 - r_0 e^{(-t/\tau_r)}]e^{(-t/\tau_f)} \quad (2a)$$

$$Y_p(t) = A_p + B_p[1 + 2r_0 e^{(-t/\tau_r)}]e^{(-t/\tau_f)} \quad (2b)$$

The fluorescence lifetime (τ_f), rotational reorientation time (τ_r), and initial anisotropy (r_0) were held common in both of the decays.

2.2. Impulse Reconvolution Anisotropy Analysis. The impulse reconvolution model decay law is defined by the more generalized form

$$r(t) = r_\infty + B_1 e^{(-t/\tau_{r1})} + B_2 e^{(-t/\tau_{r2})} \quad (3)$$

For $t = 0$, the above equation becomes $r_0 = R_\infty + B_1 + B_2$, where r_0 stands for the zero-time or fundamental anisotropy and r_∞ represents the limiting anisotropy at long time after pulse excitation.

However, in cases that a direct fitting procedure to the $r(t)$ data points is technically impossible, because the pulse width is comparable to the decay times, then the analysis of data should be done in two separate parts, making use of the definition form of fluorescence anisotropy: first, analysis of the anisotropy sum data ($S(t)$) to extract fluorescence decays and produce an *impulse response function*, via the standard exponential fitting procedure, and second, analysis of the anisotropy difference data ($D(t)$) to extract up to two rotational decay components via the impulse reconvolution fitting, with the fit constrained by the fluorescence *impulse response function*.

$$D(t) = r(t)\,S(t) = [r_\infty + B_1 e^{(-t/\tau_{r1})} + B_2 e^{(-t/\tau_{r2})}]S(t) \quad (4)$$

The goodness of fit was judged by various statistical considerations such as reduced chi-square values close to unity and a random distribution of weighted residuals.

3. Results and Discussion

3.1. Spectroscopic Aspects of PPD. Steady-state absorption and emission spectra of PPD at room temperature show little solvent dependence of peak positions and Stokes shifts (variations within 3 nm). Furthermore, the fluorescence quantum yields of PPD at room temperature were measured to be 0.76 in cyclohexane, 0.83 in ethanol, 0.82 in ethylene glycol, 0.83 in 40/60 v/v ethylene glycol/water, and 0.85 in net water. In the fluorescence lifetime measurements, all fluorescence decays could be adequately fitted by the convolution of single-exponential model functions with the instrument response. It should be pointed out that the singlet state of PPD decays with a fluorescence lifetime that does not exhibit any noticeable solvent dependence. Recovered lifetimes were 1.0 ns for cyclohexane, 1.24 ns for ethanol, 1.27 ns for ethylene glycol, 1.29 ns for 40/60 v/v ethylene glycol/water, and 1.29 ns for water.

3.2. Orientational Relaxation Dynamics. According to the modified Stokes−Einstein−Debye (SED) hydrodynamic theory,[22] the rotational reorientation time (τ_r) for a probe molecule is given by

$$\tau_r = (fC)\frac{\eta V}{k_B T} \quad (5)$$

where V is the molecular volume of the probe, η is the viscosity of the solvent, κ_B is the Boltzmann constant, T is the absolute temperature, f is the shape factor and is well specified, and C is the boundary condition parameter dependent strongly on solute, solvent, and concentration. Depending on the probe and solvent system, the boundary condition can be either of stick or slip type.[22] In the first approximation, namely, the stick limit, the first solvent shell coherently rotates with the probe molecule or alternatively there is a strong coupling between solute and solvent molecules along the surface tangent. In this case, the parameter C is set equal to unity and is valid when the size of the rotating probe is considerably larger than that of the solvent molecules. In the other level of approximation of rotation diffusion known as the slip limit, the solvent is assumed not to rotate with the probe molecule and is applicable for solute molecules whose size is comparable to or less than that of solvent molecules. In such a case, the value of C could be close to zero when the boundary condition is considered to be perfectly slip. For probe molecules having a size comparable to that of the solvent molecules, the value of C can be within $0 < C < 1$, which is the intermediate case between stick and slip boundary conditions. Since the size of PPD is much bigger than that of water molecules, it is expected that the probe in aqueous solution will follow the stick boundary condition (vide infra). An analogous situation has been frequently adopted in studies concerning solutes of comparable size to PPD.[23−28]

The solute PPD can be modeled as a prolate ellipsoid. The choice of a prolate model has been based on the fact that (i) the transition dipole $S_0 \rightarrow S_1$ is along the major molecular axis, as derived from calculations[29] and confirmed experimentally[30] by rotational coherence spectroscopy, and (ii) the emission transition moment is also collinear with the major molecular axis, as manifested in the present work; specifically, in a time-resolved fluorescence anisotropy experiment of PPD in ethylene glycol at room temperature using the impulse reconvolution method, the recovered limiting anisotropy at $t = 0$ (r_0) approached the value 0.39 which is, within experimental error, equal to that predicted for the perfect parallel orientation ($r_0 = 0.4$) between absorption and emission dipoles. Consequently, the rotation or spinning about the long axis does not displace the collinear transition moments and anisotropy persists. Thus, the only contribution to the measured anisotropy decay will be from rotation perpendicular to the symmetry axis. In the case of a prolate model, the stick rotational diffusion time (τ_r) is given by[31]

$$\tau_r = \frac{2(\rho^2+1)(\rho^2-1)^{3/2}}{3\rho[(2\rho^2-1)\ln\{\rho + (\rho^2-1)^{1/2}\} - \rho(\rho^2-1)^{1/2}]}\frac{\eta V}{k_B T} \quad (6)$$

where V is evaluated from the method of van der Waals increments[32] and ρ is the ratio of the longitudinal semiaxis α to the equatorial semiaxis b of the ellipsoid. The hydrodynamic volume of PPD was calculated to be 202 Å^3 by a new fast method termed atomic and bond contributions of van der Waals volume (VABC).[32] The longitudinal semiaxis of the spheroid is taken as half of the length along the long axis ($\alpha = 7.35$ Å) after geometry optimization using the PM3 semiempirical method; the minor axis ($b = 3.64$ Å) is then determined by equating the volume of the spheroid to be equal to the van der Waals volume of the solute.

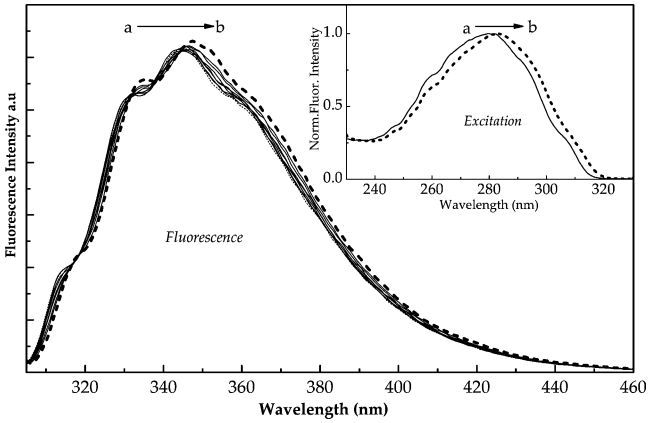

Figure 1. Fluorescence spectra of PPD (3.4 μM) in aqueous solution with varying concentrations of α-CD (λ_{exc} = 297 nm). The concentrations of α-CD at the start and end of titration are (a) 0.0 M and (b) 20 mM. For details relating to intermediate concentrations, see Figure 2. Inset: Excitation fluorescence spectra in the presence of (a) 0.0 M and (b) 20 mM α-CD. The emission monochromator was centered at 350 nm.

According to eq 6 and by setting V = 202 Å^3, $\rho = \alpha/b$ = 7.35 Å/3.64 Å = 2.02, the predicted rotational correlation time for PPD in water at 23 °C (viscosity η = 0.93 cP) is calculated to be τ_r = 69 ps under stick boundary conditions. Because of the limited time resolution (~100 ps) of our single-photon counter instrument, we were unable to directly measure this fast depolarization decay component. However, by introducing r_{ss} = 0.018 and τ_f = 1.29 ns into the Perrin equation,[22] the rotational correlation time of PPD in net water was estimated to be τ_r = 63 ps. Interestingly, the experimentally estimated value τ_r = 63 ps is very close to the one calculated for stick boundary approximation τ_r = 69 ps, as suggested previously.

3.3. The Case of α-CD. When an aqueous solution of PPD (3.4 μM) is titrated with α-CD, the fluorescence spectra of PPD (exc. at 297 nm) undergo a systematic, albeit weak, red shift with increasing CD concentration, while several isoemissive points at 318, 332, 338, and 344 nm appear. It should be pointed out that the overall changes proceed nearly without any augmentation or loss of total quantum yield (free and complexed PPD). Fluorescence lifetime measurements, on the other hand, do not reveal any significant perturbation between free and complexed dye. In fact, the fluorescence decays of the first electronic state of PPD, both in pure water and in the presence of an excess (2×10^{-2} M) of α-CD, can be fitted reasonably well with a single-exponential function with lifetimes of 1.29 ± 0.01 and 1.41 ± 0.01 ns, respectively. Moreover, ground-state absorption spectra of PPD (not shown) remain almost invariable as the concentration of α-CD increases at least at excitation wavelengths around 300 nm (the variation of optical density was within experimental error, less than 10^{-3}). The fluorescence excitation spectrum of PPD, however, monitored in the presence of 20 mM of α-CD shows a marked red shift with respect to that observed in pure water (see the inset of Figure 1).

The small red shift detected in the fluorescence spectra of PPD in the presence of α-CD has been widely observed in numerous studies dealing with complexation between chromophoric systems and cyclodextrins.[23,25,33−35] The explanation is based on the fact that, upon complexation, the local solvation environment changes in a way that is similar to changing the solvent from water to a less protic one.[25] The nature of the red shift in the present work was further explored by studying the excitation and fluorescence spectra of PPD in different solvents

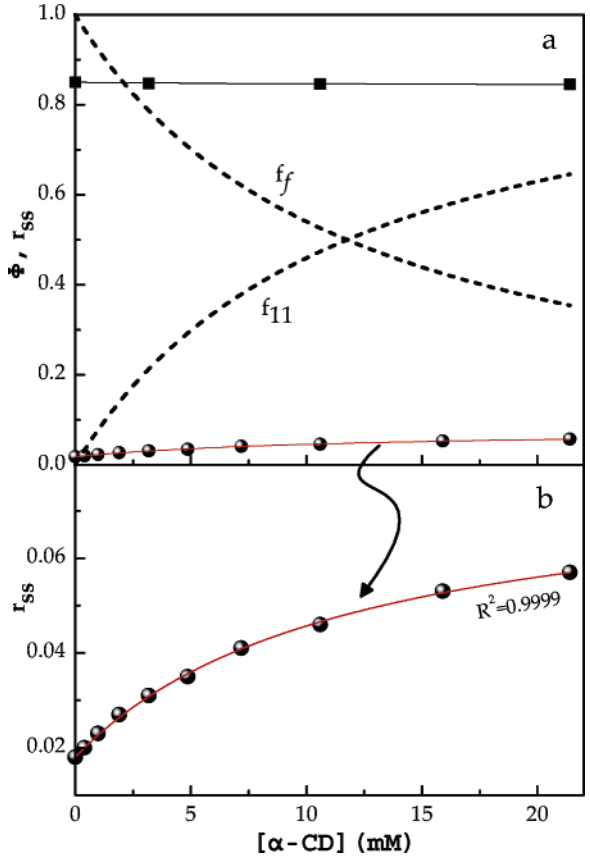

Figure 2. Computer fits (red lines) of eq 8 to the Φ vs [α-CD] experimental data (■) and of eq 10 to the r_{ss} vs [α-CD] experimental data (●) for PPD (3.4 μM; λ_{exc} = 297 nm). The dashed lines represent the molar fractions of free (f_f) and complexed (f_{11}) solute as derived from best fitting parameters (see also Table 1).

(not shown). Indeed, both spectra show that as one proceeds from water to ethanol and cyclohexane solvent, a red shift occurs in the fluorescence spectra, which does not exceed 3 nm.

It should be noticed, however, that in the overwhelming majority of analogous systems, namely, fluorophores and CDs, the observed shift in their fluorescence spectra is usually accompanied by significant changes in fluorescence quantum yield and lifetime. The locally excited state of PPD, however, does not show any sensitivity to the polarity and viscosity of the medium, as mentioned previously (see section 3.1). Therefore, in the absence of aggregation phenomena, the information provided by the nearly flat Φ and τ versus [CD$_s$] is poor and may lead to erroneous conclusions.[36] If such a case were to occur, one might expect that, besides environmental changes induced by complexation with CDs, significant alteration of the rotational relaxation time of the "caged" PPD would appear; and this because the complex usually rotates as a whole, with a relaxation time much longer than that observed for free solute in net water.[37] Consequently, both steady-state (SS) and time-resolved (TR) fluorescence anisotropy are the most powerful fluorescence parameters to elucidate complexation aspects between PPD and cyclodextrins.[16,23,25]

Figure 2a shows the variation of the fluorescence quantum yield (Φ) and steady-state anisotropy (r_{ss}) as the concentration of added α-CD increases while keeping constant the concentration of PPD dye, namely, 3.4 μM (λ_{exc} = 297 nm). As can be clearly seen, the quantum yield (Φ) is nearly invariable over the entire concentration region studied. The fluorescence anisotropy (r_{ss}), however, shows quite discriminating characteristics (Figure 2b). It starts from a value of 0.018 for free PPD and

then rises systematically; even in the presence of the highest concentration of α-CD employed (21.4 mM), it does not level off. From a qualitative point of view, this means that complete complexation of the solute was not achieved even at a concentration ratio of 1:6300 (PPD/α-CD). Quantitatively, the complexation scheme and the association constant(s) for the PPD/α-CD system were determined by analyzing r_{ss} versus [α-CD].

In the case of a 1:1 complex formed between PPD and α-CD, the equilibrium can be written as

$$\text{PPD} + \alpha\text{-CD} \overset{K_1}{\rightleftharpoons} \text{DPP}-\alpha\text{-CD} \tag{7}$$

The total fluorescence quantum yield at any moment during the titration procedure is given by[16]

$$\Phi = f_f\Phi_f + f_{11}\Phi_{11} \tag{8}$$

where Φ_f, $f_f = [\text{PPD}]/[\text{PPD}]_{tot}$ and Φ_{11}, $f_{11} = [\text{PPD}-\alpha\text{-CD}]/[\text{PPD}]_{tot}$ represent the quantum yield and the molar fraction of the free and bound PPD, respectively. Notice that the above equation (eq 8) is valid when the optical density, at the excitation wavelength, remains constant by CD titration, for example, an isosbestic point. Recall again that in the present case variation of the optical density at 297 nm was less than 10^{-3} and therefore eq 8 is applicable.

By analogy, the fitting equation r_{ss} versus [α-CD] can be written as[16]

$$r_{ss} = I_f r_f + I_{11} r_{11} \tag{9}$$

where r_{ss} is the total measured anisotropy, whereas I_f and I_{11} refer to the fraction of the total fluorescence intensity due to the free and complexed PPD molecule, respectively.

The intensity fractions can be expressed as $I_f = f_f\Phi_f/\Phi$ and $I_{11} = f_{11}\Phi_{11}/\Phi$; Φ_f/Φ and Φ_{11}/Φ represent the ratio of the quantum yield of the free and complexed dye form. Then, and taking into account the Perrin equation for the *overall* tumbling motion ($\tau^{ov}_{r(11)}$) of the dye in the complexed state, the above equation rearranges to

$$r_{ss} = f_f\frac{\Phi_f}{\Phi}r_f + f_{11}\frac{\Phi_{11}}{\Phi}r_{11} \tag{10}$$

with

$$r_{11} = r_0/(1 + \tau_{f(11)}/\tau^{ov}_{r(11)}) \tag{11}$$

Notice that the master fitting equation (eq 10) contains the parameters r_f, r_0, and τ_f which are known quantities, since they can be individually measured. The connection between the unknown concentration of the species which participate in the equilibrium during the titration, namely, PPD and PPD/α-CD, and the corresponding binding constant K_{11} (fitting parameter) is made using eq 11a and the balance of mass for PPD (11b).

$$[\text{PPD}-\alpha\text{-CD}] = K_{11}[\text{PPD}][\alpha\text{-CD}] \tag{11a}$$

$$[\text{PPD}]_{tot} = [\text{PPD}] + [\text{PPD}-\alpha\text{-CD}] \tag{11b}$$

These equations can easily combine to give

$$[\text{PPD}] = \frac{[\text{PPD}]_{tot}}{1 + K_{11}[\alpha\text{-CD}]} \tag{12a}$$

and

$$[\text{PPD}-\alpha\text{-CD}] = K_{11}\frac{[\text{PPD}]_{tot}}{1 + K_{11}[\alpha\text{-CD}]}[\alpha\text{-CD}] \tag{12b}$$

We can further assume that the free and analytical concentration (total) of α-CD are equal at any stage of titration, namely, $[\alpha\text{-CD}] \approx [\alpha\text{-CD}]_{tot}$; this appears to be a valid approximation, since a large excess of α-CD relative to PPD was used.

Hence, the unknown concentrations of PPD and PPD/α-CD and consequently the molar fractions f_f and f_{11} can be expressed as a function of the known quantities [α-CD] and $[\text{PPD}]_{tot}$ and the desired parameter K_{11}. Finally, introducing the known quantities $r_f = 0.018$, $r_0 = 0.39$, and $\tau_{f(11)} = 1.41$ ns as fixed parameters and allowing K_{11}, Φ_{11}, and $\tau^{ov}_{r(11)}$ as free-running parameters, a simultaneous fit for both Φ and r_{ss} versus [α-CD] (eqs 8 and 10, respectively) was performed. The obtained values were $K_{11} = 85 \pm 4\ \text{M}^{-1}$, $\Phi_{11} = 0.84 \pm 0.001$, and $\tau^{ov}_{r(11)} = 360 \pm 10$ ps with an excellent satisfactory criterion for their goodness of fits ($R^2 = 0.9999$).

On the basis of steady-state anisotropy alone, one cannot directly evaluate the full scheme of rotational relaxation dynamics (τ_r) of a solute caged in a nanocavity (i.e., a global motion of the nanostructure with an internal motion of the guest; see also the case of β-CD). This is because measured values of r_{ss} represent an average of the anisotropy decay over the intensity decay,[18] and therefore, only an *overall* rotational reorientation time ($\tau^{ov}_{r(11)}$) is observed. To this end, we performed time-resolved fluorescence anisotropy experiments and we have compared the results with those obtained indirectly from r_{ss} versus [α-CD].

Typical fits to the experimental data obtained from an aqueous solution of 3.4 μM PPD containing 20 mM α-CD at 23 °C using both the spherical rotor anisotropy (SRA) model and impulse reconvolution analysis (IRA) are shown in Figures 3 and 4, respectively. Both models are fitted very satisfactorily with a monoexponential function, as indicated from the goodness of the fits (see also Table 1). The evaluated parameters were $\tau^{gl}_{r(11)} = 380 \pm 23$ ps, $\tau_{f(11)} = 1.41$ ns, and $r_0 = 0.28 \pm 0.01$ ($\chi^2 = 1.130$) for the former one and $\tau^{gl}_{r(11)} = 370 \pm 40$ ps, $r_\infty \approx 0$, and $r_0 = 0.25 \pm 0.01$ ($\chi^2 = 1.05$) for the latter one. It is worth noticing that the rotational relaxation times ($\tau_{r(11)}$) measured from both models are, within experimental error, equal (see Table 1) and directly reflect the global motion of the complex, $\tau^{gl}_{r(11)}$, as will be clear in section 3.4. Furthermore, they, namely, $\tau^{gl}_{r(11)}$, nearly coincide with the one ($\tau^{ov}_{r(11)} = 360 \pm 10$ ps) which has been independently evaluated from static anisotropy experiments, namely, r_{ss} versus [α-CD] (see Table 1).

Before proceeding further, however, we wish to clarify another point relating to the zero-time or fundamental anisotropy (r_0) as well as to the observed single-exponential behavior of the above fits. In both models, namely, SRA and IRA, r_0 decreased from 0.39 to about 0.26; this means that an additional fast depolarization process on a time scale below the time resolution of 100 ps of the single-photon counter apparatus employed in this work takes place.[38] As manifested from the analysis of r_{ss} versus [α-CD], even in the presence of 20 mM α-CD, namely, a concentration ratio of 1:5880 (PPD/α-CD), about 35% of the total PPD population still holds the aqueous bulk phase (see the molar fractions in Figure 2). Therefore, one would expect that the partial loss of the zero-time anisotropy $r_0 = 0.39$ may be related to the depolarization induced from rotation of the free dye itself; recall again that PPD in water at 23 °C rotates on a time scale ($\tau_r = 63$ ps) which is faster than the instrument time resolution (100 ps) and therefore its contribution to the total decay trace is missed.

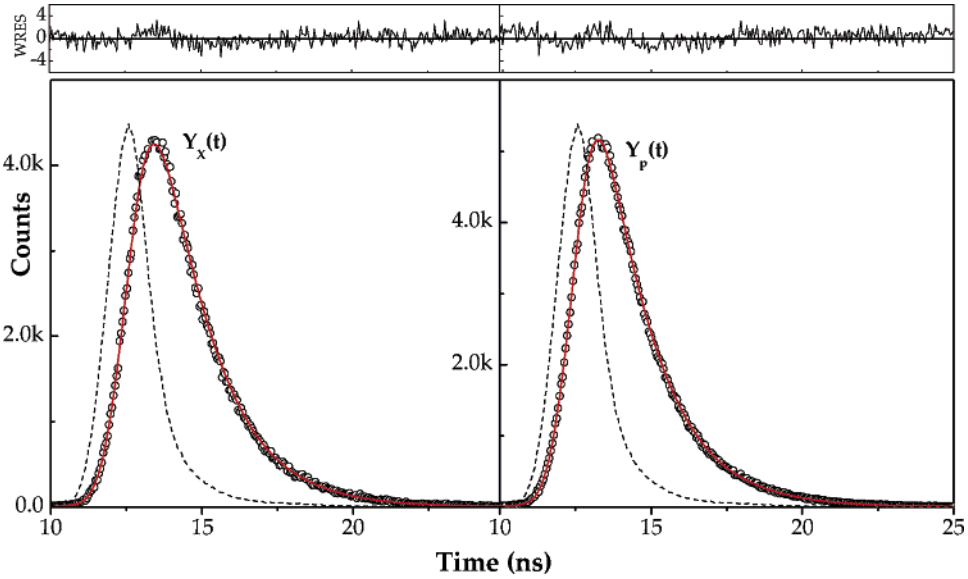

Figure 3. Spherical rotor anisotropy model: Simultaneous fit of both the crossed (left) and parallel (right) decay components of an aqueous solution of PPD (3.4 μM) containing 2.0 mM α-CD at 23 °C; $\lambda_{exc} = 303$ nm. The solid and dashed lines represent the best fitting curve and instrument response function, respectively; the parameters evaluated were $\tau^{gl}_{r(11)} = 380 \pm 23$ ps, $\tau_{f(11)} = 1.41$ ns, and $r_0 = 0.28 \pm 0.01$ ($\chi^2 = 1.130$). The corresponding weighted residuals (WRES) are given on top for each curve.

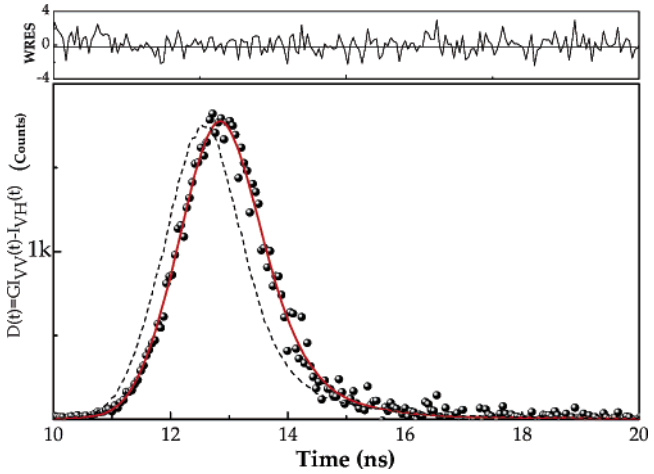

Figure 4. Impulse reconvolution anisotrpoy analysis (IRA) of an aqueous solution of PPD (3.4 μM) containing 2.0 mM α-CD at 23 °C (for details, see experimental part); $\lambda_{exc} = 303$ nm. The solid (red) and dashed lines represent the best fitting curve and instrument response function, respectively; the evaluated parameters were $\tau^{gl}_{r(11)} = 370 \pm 40$ ps, $r_\infty \approx 0$, and $r_0 = 0.25 \pm 0.01$ ($\chi^2 = 1.05$). The corresponding weighted residuals (WRES) are given on top.

To further verify the structure of the rotating species with a reorientation relaxation time of ~370 ps, we took into consideration the geometrical characteristics of the reactants: the internal diameter of the α-CD is 4.7−5.7 Å and its length is ~8 Å;[9d] on the other hand, the dimensions of PPD are 14.7:6.7:3.4 Å (including vdW radii). Furthermore, it is generally accepted that only one phenyl ring is able to penetrate the small cavity of α-CD; thus, the rest of the molecule is reasonably outside the cavity.[39] Therefore, the model of the prolate ellipsoid is quite appropriate for such a representative structure in which a significant portion of the dye (~70%) remains extended out of the CD cavity (Scheme 2).

Then, by introducing $V = 1125$ Å^3 as the global volume of the aforementioned complex, $\rho = a/b \sim 10$ Å/7.5 Å ~ 1.34, into eq 6, the overall rotational reorientation time is estimated to be 307 ps in very good agreement with the one (370 ± 40 ps) evaluated from our SS and TR fluorescence experiments. This also agrees with the results obtained by means of ^{2}H and ^{13}C nuclear relaxation,[37] which reveal that upon inclusion with α-CD the rotational reorientation times of the substrates increase by a factor ~4.

Finally, the case of two α-CDs that include a dye molecule in the tail-to-tail orientation, namely, 1:2 complex between PPD and α-CD, is not supported from our findings. Recently, for the 1:2 complex between 1′-hydroxyl-2′-acetonaphone and α-CD, a global rotational time of ~950 ps that exceeds more than twice that of this work (~370 ps) has been reported.[40]

3.4. The Case of *β*-CD. The situation with respect to spectral changes of PPD induced by complexation with β-CD does not differentiate considerably in comparison with α-CD. Figure 5 shows the variation of the fluorescence quantum yield (Φ) and steady-state anisotropy (r_{ss}), as the concentration of added β-CD increases, while keeping constant the concentration of PPD dye (3.4 μM). As can be seen, the quantum yield (Φ) shows a little decrease as the concentration of β-CD increases. It was found also that the fluorescence lifetime undergoes a very subtle change and remains nearly invariable ($\tau_f = 1.46$ ns) close to the titration limit (10 mM). The static fluorescence anisotropy (r_{ss}) versus [β-CD], however, shows quite distinct and interesting features compared to that observed with α-CD. It rises rather sharply in the start, indicating stronger binding than its α-CD analogue, and then tends to level off as the β-CD concentration approaches ~10 mM.

Fitting of eq 10 linked with eq 8 (Figure 5) to the above data produces a very satisfactory goodness of fit ($R^2 = 0.9999$), as may be seen in the results summarized in Table 2. Contrary to what was observed in the case of α-CD, the derived rotational reorientation time which accounts for the *overall* tumbling motion $\tau^{ov}_{r(11)} = 284 \pm 20$ ps of the dye embedded in the β-CD cavity does not agree with the one, $\tau^{gl}_{r(11)} = 480 \pm 30$ ps, evaluated from time-resolved experiments (see Table 2). Therefore, the question that arises is "what does cause this underestimation of $\tau^{ov}_{r(11)}$ whose value appears to be even lower than that ($\tau^{ov}_{r(11)} = 360 \pm 10$ ps) of the smaller α-CD molecule?" Recall again that in a time-resolved anisotropy experiment one normally observes directly, from a dynamic point of view, each independent depolarization process,[17]

TABLE 1: Recovered Fluorescence Anisotropy Parameters of PPD (3.4 μM) in the Presence of 20 mM α-CD at 23 °C (Values Are the Average of Five Independent Experiments) and Binding Constant (K_{11}) and Fluorescence Parameters for the Complex PPD/α-CD, Obtained from r_{ss} vs [α-CD] at 23 °C

		$\tau^{gl}_{r(11)}$ (ps)	r_0	r_∞	τ_f (ns)	χ^2
spherical rotor anisotropy (SRA) model		380 ± 23	0.28 ± 0.01	≅0	1.41 ± 0.005	1.13
impulse reconvolution analysis (IRA)	1-exp. term	370 ± 40	0.25 ± 0.01	≅0		1.05

r_{ss} vs [α-CD]	K_{11} (M^{-1})	Φ_{11}	$\tau^{ov}_{r(11)}$ (ps)	τ_f (ns)	R^2
eq 10	85 ± 4	0.84 ± 0.001	360 ± 10	1.4[a]	0.9999

[a] Measured independently and introduced as fixed.

SCHEME 2: Schematic Representation of the α-CD/PPD Inclusion Complex

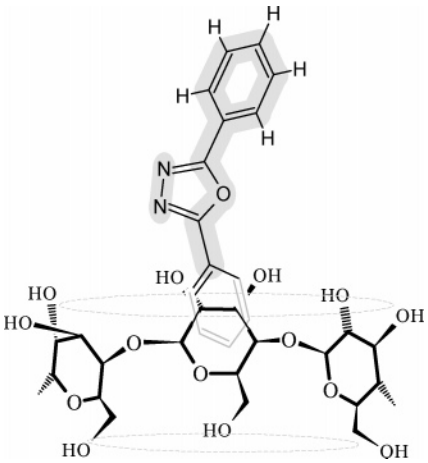

expressed in terms of reorientation relaxation (τ_r). However, in a steady-state fluorescence anisotropy experiment, the overall relaxation (τ_r^{ov}) calculated indirectly from the Perrin equation may reflect a mean value of more than one depolarization process, that is, the tumbling motion of a global host/guest nanostructure with a concomitant internal librational motion of the guest inside the host cavity.

Therefore, the evaluated $\tau^{ov}_{r(11)} = 284 \pm 20$ ps from r_{ss} versus [β-CD] does not manifest itself as being representative of an exclusive global motion of the 1:1 complex or it contains and contribution of independent internal guest motion inside the β-CD cavity. To test this assertion, we have reconstructed the master fitting equation (eq 10) as follows: According to Soleillet's rule[18] which states that the anisotropy can be expressed as a product of the various depolarization factors that occur in a given sample, we have split the r_{11} expression into two parts (eq 13); the first one stands for the loss of anisotropy due to the *global* rotation of the nanostructure, namely, the 1:1 complex, whereas the second one accounts for the average angular displacement (θ) of the dye into the cavity during its excited-state lifetime.

$$r_{11} = r_0 \frac{1}{1 + \tau_{f(11)}/\tau^{gl}_{r(11)}} \frac{3\langle\cos^2\theta\rangle - 1}{2} \qquad (13)$$

Introducing this modified term to the master equation (eq 10), we have performed several simulations to check the validity and sensitivity of the new equation to the recovered parameters. We found that, by fixing $\theta = 27.5°$, the fitting was very successful ($R^2 = 0.9999$), giving among other parameters $\tau^{gl}_{r(11)} = 480 \pm 12$ ps, which matches the one being evaluated from time-resolved anisotropy (see Table 2). It is worthwhile to mention that a very narrow range of θ values ($26° \le \theta \le 29°$) creates acceptable fits, reproducing the parameter $\tau_{r(11)}$ within its own experimental error, 480 ± 30 ps, as derived from TRFA analysis; the rest of the fitting parameters, namely, K_{11} and Φ_{11} are not essentially affected. Moreover, attempts to fit the experimental data, ignoring internal rotation ($\theta = 0°$) and keeping $\tau^{gl}_{r(11)} = 480$ ps fixed, have dramatically failed, as seen in Figure 5. Finally, higher-order complexes, that is, 1:2 PPD/β-CD were not detected as in the previous case of α-CD.

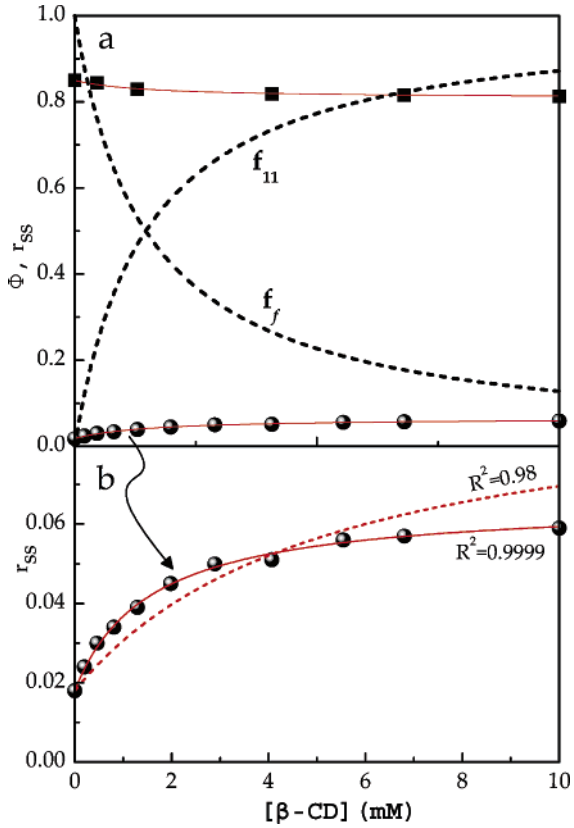

Figure 5. (a) Computer fits (red lines) of eq 8 to the Φ vs [β-CD] experimental data (■) and of eq 10 modified with eq 13 to the r_{ss} vs [β-CD] experimental data (●) for PPD (3.4 μM); $\lambda_{exc} = 297$ nm. The dashed lines (upper panel) represent the molar fractions of free (f_f) and complexed (f_{11}) solute as derived from best fitting parameters (see also Table 2). The dashed line in the lower panel represents the best fitting curve to eq 10 by fixing $\tau^{ov}_{r(11)} = 480$ ps obtained from TRFA experiments (see text and Table 2 for details).

Balabai et al.[23] have measured the rotational relaxation time of three different probe molecules encapsulated to β-CD in aqueous solution, namely, resorufin, oxazine-118, and oxazine-725. They reported reorientation times of 301, 281, and 406 ps, respectively, for the global tumbling motion of the complexes. For resorufin/β-CD and oxazine-118/β-CD complexes, however, they were able to observe an additional fast depolarization component of ~58 ps which was assigned as being responsible for an independent internal motion—as fast as that in net water—of the probe molecules inside the β-CD cavity.

TABLE 2: Recovered Fluorescence Anisotropy Parameters of PPD (3.4 μM) in the Presence of 10 mM β-CD at 23 °C (Values Are the Average of Five Independent Experiments) and Binding Constant and Fluorescence Parameters Obtained from r_{ss} vs [β-CD] at 23 °C

		$\tau^{gl}_{r(11)}$ (ps)	r_0	r_∞	τ_f (ns)	χ^2
spherical rotor anisotropy (SRA) model		484 ± 22	0.29 ± 0.01	≅0	1.46 ± 0.005	1.12
impulse reconvolution analysis (IRA)	1-exp. term	476 ± 35	0.26 ± 0.01	≅0		1.04

r_{ss} vs [β-CD]	K_{11} (M^{-1})	Φ_{11}	θ_c (deg)	$\tau^{ov}_{r(11)}$ (ps)	τ_f (ns)	R^2
eq 10	681 ± 60	0.808 ± 0.002		284 ± 20	1.46[b]	0.9999
eq 10	207 ± 21	0.785 ± 0.008		480[c]	1.46[b]	0.985
modified eq 10 with eq 13	682 ± 60	0.808 ± 0.001	27.5[a]	480 ± 12	1.46[b]	0.9999

[a] Was kept fixed. [b] Measured independently and introduced as fixed. [c] Obtained from time-resolved analysis and introduced as fixed.

Most recently, Tormo et al.[26] have also detected a free motion of the guest methyl 2-amino-4,5-dimethoxy benzoate into the β-CD nanocavity with a rotation relaxation time of ~53 ps similar to that observed in pure tetrahydrofurane; they also found that the global motion of the confined 1:1 complex is governed by a rotational relaxation time of 510 ps. From the above investigations as well as the compatibility of PPD size with that of the aforementioned probes, free rotation of PPD to a cone angle into the β-CD cavity is not unlikely to occur; in such a case, it is expected to decay with $\tau_r \sim 60$ ps which is below the instrument response and does not contribute to the total decay trace. Finally, the estimated value $\tau^{gl}_{r(11)} = 480 \pm 30$ ps for the global motion of the PPD/β-CD adduct is of the same order of magnitude as the experimental ones found from other investigators.[23,26]

3.5. The Case of γ-CD. Contrary to the results obtained for α- and β-CD, PPD shows very different spectroscopic behavior in the presence of γ-CD. When γ-CD is added progressively to an aqueous solution containing 5.4 μM PPD, there is a systematic dropping and slight broadening of the PPD absorption spectrum (not shown); at the same time, the fluorescence quantum yield decreases noticeably and in the emission spectrum a new, red-shifted excimer-like emission band gradually appears and is visible as a red tail to the fluorescence spectrum (see Figure 6a). Interestingly, the steady-state anisotropy (r_{ss}) does not remain flat across the emission spectrum (see the inset of Figure 6a), showing an upward tendency toward the red tail of the spectrum, while its gradient effectively increases with increasing γ-CD concentration (not shown). The above findings strongly support interacting couples of PPD in the ground state and the existence of more than one emissive state of PPD in the presence of γ-CD.

To further investigate and clarify the behavior of PPD in the presence of γ-CD, we performed detailed time-resolved fluorescence experiments. The gated time-resolved spectra recorded for an aqueous solution of PPD (5.4 μM) containing 26.5 mM γ-CD are shown in Figure 6b. The early-gated spectrum A, which corresponds to fluorescence emitted during the first 1.5−3.1 ns, consists principally of the locally excited state emission, namely, free PPD and singly occupied complexes (DPP/γ-CD). At longer times following pulse excitation $7.8 \leq \Delta t \leq 9.5$ ns, the emission is governed by a new broad emission band, D_1, centered at 347 nm which in the late-gated spectrum ($\Delta t \geq 18$ ns) almost disappears while a new structureless emission band with a maximum at 355 nm is observed. The identification and kinetics of all emitting species was further studied by analyzing fluorescence decay traces at various emission wavelengths; the fitting parameters and goodness of fits are given in Table 3.

The decay curve monitored at the red tail of the fluorescence spectrum (440 nm) was analyzed as a triple-exponential decay consisting of two long-living components, D_2 ($\tau_4 = 11.4 \pm 2$ ns) and D_1 ($\tau_3 = 3.9 \pm 0.3$ ns), and a "normal" A ($\tau_2 = 1.41$ ns) decaying component. By entering gradually into the intermediate wavelengths of the spectral region (415, 380, and 350 nm, respectively), the normal decaying component A gains percentage at the expense of the D_1 and D_2, while an additional fast component ($\tau_1 \cong 320$ ps) contributes to the fluorescence decay whose percentage increases toward the shorter wavelengths. Finally, at the high-energy band of the spectrum (320 nm), both the fast ($\tau_1 \cong 320$ ps) and the normal A ($\tau_2 = 1.41$ ns) decaying components represent the total decay trace, with only a minor 11% contribution of the D_1 ($\tau_3 = 3.9 \pm 0.3$ ns) species. In conformity with the gated time-resolved spectra, the formation of two types of excimers is demonstrated by analyzing the decay traces. One is the long-living excimer D_2 ($\tau_4 = 11.4$ ns, $\lambda_{max} = 355$ nm) observed at the late-gated spectrum ($\Delta t \geq 18$ ns) of the time-resolved spectra (see Figure 6b); the other is

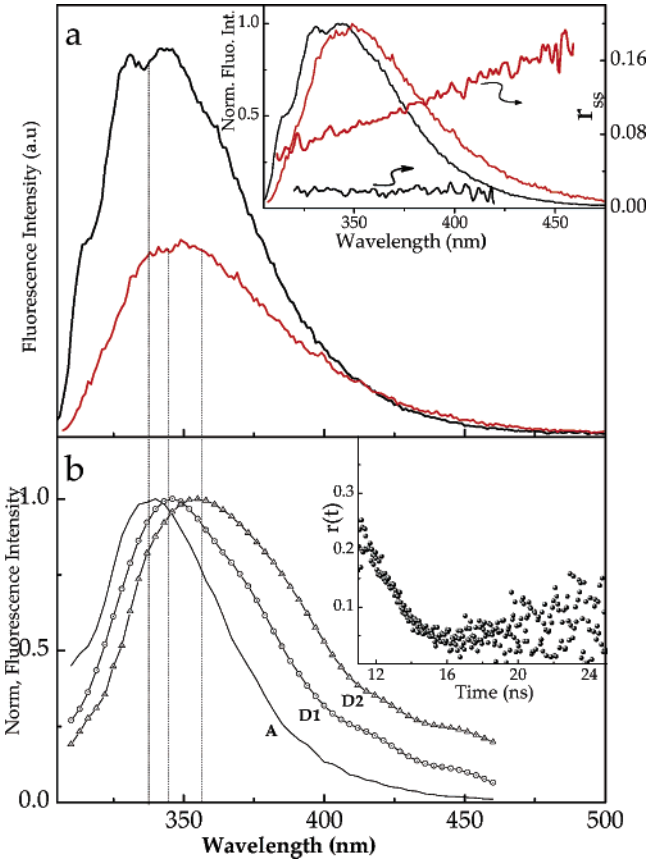

Figure 6. (a) Fluorescence spectra of PPD (5.4 μM) in water before (black line) and after (red line) the addition of 26.5 mM γ-CD. Inset: Normalized static fluorescence spectra as above, together with their corresponding fluorescence anisotropies (r_{ss}). (b) Gated time-resolved spectra of the latter solution; the gate times of spectra A, D_1, and D_2 are 1.5−3.1, 7.8−9.5, and 18 nm, respectively; a smoothing was applied to the last spectrum due to its low signal. Inset: Anisotropy decay ($r(t)$) upon excitation at 303 nm and observation at 350 nm.

TABLE 3: Recovered Decay Times (τ, ns) and Percentages (% τ) of the Emitting Species in an Aqueous 2.65 mM γ-CD Solution Containing 5.4 μM PPD at Various Wavelengths (nm)

emission wavelength	τ_1	τ_2	τ_3	τ_4	% τ_1	% τ_2	% τ_3	% τ_4	χ^2
440		1.41 ± 0.05	3.7 ± 0.3	11.4 ± 2		52	42	6	1.11
415	0.32 ± 0.03	1.46 ± 0.05	3.9 ± 0.3	11.4 ± 2	3	61	33	3	1.05
380	0.32 ± 0.03	1.48 ± 0.03	3.9 ± 0.3	11.4 ± 2	5	70	24	1	1.07
350	0.34 ± 0.03	1.43 ± 0.02	3.9 ± 0.2		7	72	21		1.04
320	0.33 ± 0.03	1.44 ± 0.02	3.7 ± 0.2		8	81	11		0.997

[a] The analysis of the fluorescence decay traces was made by using exponential curve fitting of three or four exponential terms. The statistical parameter χ^2 is given in the last column.

the shorter-living excimer D_1 ($\tau_3 \cong 4$ ns, $\lambda_{max} = 347$ nm) which has a major contribution at intermediate times of 7.8 ns $\leq \Delta t \leq 9.5$ ns after pulse excitation. The normal decaying component A ($\tau_2 = 1.41$ ns) could be assigned as the locally excited state of PPD arising from singly occupied complexes and PPD dispersed in the aqueous phase, as previously discussed in detail. Finally, the fast decaying component ($\tau_1 \cong 320$ ps) which contributes to the fluorescence decay in the spectrum region where the locally excited state emits and also appears only when excimer emission is present should be consistent with the rapid trapping of the initially formed singlet exciton at the preformed excimer-like dimer configuration. In other words, during 0−320 ps, the photoexcited dimer is changed into the excimer state.[41,42] Alternatively, this fast component could be observed directly as a rising part in the decay profile into the excimeric spectral region, but unfortunately, due to the multiexponential behavior of the fluorescence decays and to limited pulse as well as to low signal/noise ratio at this wavelength region, there was uncertainty in directly detecting this fast "growing-in" component.

Dual excimer emission has been observed frequently not only in organized media in dilute solutions[42b,43] but also in the crystalline state.[44] The low-energy component has been assigned to a normal excimer with a sandwich-type arrangement of aromatic moieties, whereas the higher-energy component has been attributed to a partially overlapped pair of fluorophores. Since previous studies have shown that PPD does not produce excimers either in the solid state or in concentrated solutions,[45] it seems reasonable to adopt somewhat similar structural conformations for the D_1 and D_2 excimers observed in the present work. The remaining question is if D_1 and D_2 represent two discrete populations of dimers in which each excimer deactivates itself following a pulse excitation, or D_1 and D_2 are subsequent states of the initially excited monomer M in a preformed dimer site. In the latter case, namely, $M^* \rightarrow D_1^* \rightarrow D_2^*$, a delay in the rise time of the D_2 fluorescence equal to the decay time ($\tau_3 \sim 4$ ns) of its precursor D_1 would be observed.[46] Such a case, however, was not manifested.

In any case, the appearance of excimer formation of appropriate fluorophores in the presence of γ-CD is not a very seldom phenomenon, as has been demonstrated by us[41,47] and others.[48] It is believed that the toroidally shaped truncated cone of the wider and more flexible γ-CD constrains two guest molecules into adopting more and/or less overlapping configurations[23] suitable for excited dimer formation. It has been manifested in the literature, from a formation kinetic point of view, that the initially formed singly occupied complexes, namely, 1:1, recognize each other through intermolecular forces leading thus to a barrel-type configuration (2:2 guest/host). In the present case, however, the autonomous organization of the initially formed subunits (1:1 guest/host) is not limited to a 2:2 adduct but rather can extend to lead to big-sized nanotubular superstructures (vide infra). As mentioned before, the steady-state fluorescence anisotropy starts from a low value, that is, 0.055, and then increases monotonically on passing to the red edge of the fluorescence spectrum in which excimers are the predominant emitting species, reaching a value of ~0.18. Surprisingly, this trend proceeds in a manner opposite to what one would expect; this is because it is well-known that, for a rotating emitter, the longer the lifetime, the lesser the anisotropy.[18] Notice also that the blue part of the spectrum is governed almost exclusively by the normal A ($\tau_2 = 1.41$ ns) decaying component which was assigned to emanate from free and singly occupied complexes (1:1) between PPD and γ-CD. Indeed, the observed $r_{ss} \sim 0.055$ is of the same order of magnitude as the experimental ones which account for the 1:1 entities between PPD and α- and β-CD previously discussed. Therefore, the highly polarized fluorescence signal that demonstrates the formation of supramolecular assemblies quite larger than of simple adducts (1:1 and 2:2) originates exclusively from excimeric sites.

Unfortunately, due to the appreciable continuous change of the fluorescence anisotropy across the emission spectrum (r_{ss} vs λ (nm); see Figure 6a, inset) we were not able to directly fit r_{ss} versus [γ-CD] to evaluate the formation binding constants and the average length of these assemblies. The necessity for a flat form of r_{ss} across emission wavelengths has been pointed out with regard to the evaluation of binding constants in similar supramolecular assemblies.[16] Nevertheless, using time-resolved fluorescence anisotropy (TRFA), an estimation of the average length of these assemblies can be made. As depicted in Figure 6b (inset), the anisotropy monitored at 350 nm shows an initial decaying component while at long times does not decay to zero, as usually happens for unrestricted motions, that is, the case of α-and β-CD (see Tables 1 and 2); instead, it levels off around 0.06. By fitting the decay trace to a restricted rotor with residual anisotropy (r_∞) using impulse reconvolution analysis (IRA), a component of ~0.8 ns for the initial part of the decay and a residual anisotropy of 0.06 ± 0.01 were obtained.

$$r(t) = r_\infty + B_1 e^{(-t/\tau_{r1})} \tag{14}$$

The former may be attributed to the global motion of the nanostructure (1:1 PPD/γ-CD) in very good agreement with that ($\tau_r = 0.9$ ns) recently observed in the 1:1 adduct between 2-amino-4,5-dimethoxy benzoate and γ-CD.[26] The latter, namely, the residual anisotropy (r_∞), does not decay at least over 15 ns after pulse excitation, indicating a very large mean hydrodynamic volume of the formed adducts. It is noteworthy that the "flattening" of the $r(t)$ starts about 4 ns after the pulse, a fact which manifests that long-living fluorescence (excimers) is responsible for the flat part of the residual anisotropy, since photons from the locally excited state (~1 ns) do not contribute after 4 ns any more.

To account for an approximate down limit of the size of the nanotubular assembled adduct formed between γ-CD and PPD,

SCHEME 3: Schematic Representation of the Nanotubular Assembled Adduct Formed between γ-CD and PPD in Aqueous Solution

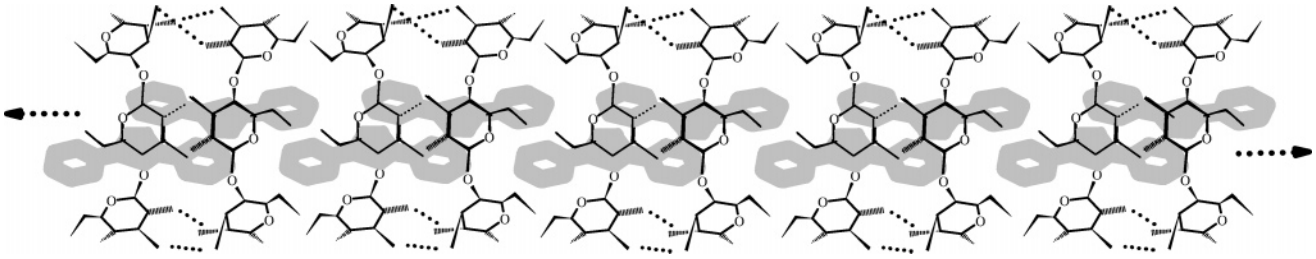

we can make use of eq 6 and the residual anisotropy as follows:[28] the nanotubular superstructure can be modeled as a prolate spheroid with semiaxis α, b, and c ($b = c \sim 9$ Å as in γ-CD alone) and volume $V = 4\pi\alpha bc/3$.[49] Introducing a value of $\tau_R > 15$ ns as the rotational relaxation time for the nanotubular entity in eq 6 and setting $\rho = \alpha/9$, one obtains $2\alpha > 134$ Å as an overall mean length for the whole entity under stick conditions; this value of the longitudinal semiaxis α corresponds to more than 17 γ-CD units per nanotube.

In summary, the vigorous changes observed when the concentration of γ-CD gradually increases in an aqueous solution containing PPD (5.4 μM), namely, significant dropping of the fluorescence quantum yield, red shifting and broadening of the emission spectra, as well as the progressive variations in the time-resolved spectra, strongly support the formation of caged interacting couples of PPD through $\pi-\pi$ aromatic interactions. Furthermore, both steady-state and time-resolved anisotropy reveal the formation of nanotubular superstructures in which dimeric forms of PPD play the role of the interlinker between γ-CD molecules (Scheme 3).

4. Conclusions

A combination of static and time-resolved fluorescence techniques is performed to explore how the relative host/guest size determines not only the structure, geometry, binding stability, and dynamic rigidity of the resulting supramolecules but also their tendency to form, through a self-assembly route, more complex supramolecular architectures.

The present results clearly demonstrate the following: (a) PPD is weakly bound, from a thermodynamic point of view, with a simple stoichiometry of 1:1 to α-CD but dynamically is tightly coupled with the ligand (α-CD) so that only a global tumbling motion was detected. (b) The next homologue β-CD interacts with PPD about an order of magnitude stronger—in terms of the thermodynamic association constant—than its smaller analogue (α-CD), but the present complex displays appreciable motion of the dye with respect to β-CD. Finally, (c) the interaction of PPD with the wider and more flexible cavity of the γ-CD gives rise to a self-associative scheme of the initially formed supramolecular building blocks, namely, singly occupied complexes (1:1), leading to big-sized nanotubular superstructures. These assemblies are recognized exclusively from dual excimer fluorescence which, in turn, is a manifestation of the *structural complementarity* between building blocks essential in the formation and stabilization of these adducts.

We believe that the results reported here are relevant and gain insight into the dynamics of supramolecular systems as well as the self-assembly/self-organization routes, which, up to now, have not been fully understood and controlled.

References and Notes

(1) (a) Lehn, J. M. *Supramolecular Chemistry: Concepts and Perspectives*; VCH: Weinheim, Germany, 1995. (b) Fujita M., Ed. *Molecular Self-Assembly*; Structure and Bonding, Vol. 96; Springer: Heidelberg, Germany, 2000. (c) Hollingsworth, M. D. *Science* **2002**, *295*, 2410−2413.

(2) Whitesides, G. M.; Grzybowski, B. *Science* **2002**, *295*, 2418.

(3) Cacialli, F.; Wilson, J. S.; Michels, J. J.; Daniel, C.; Silva, C.; Friend, R. H.; Severin, N.; Samori, P.; Rabe, J. P.; O'Connell, M. J.; Taylor, P. N.; Anderson, H. L. *Nat. Mater.* **2002**, *1*, 160.

(4) Balzani, V.; Gomez-Lopez, M.; Stoddart, J. F. *Acc. Chem. Res.* **1998**, *31*, 405.

(5) van Delden, R. A.; Koumura, N.; Harada, N.; Feringa, B. L. *Proc. Natl. Acad. Sci. U.S.A.* **2002**, *99*, 4945.

(6) (a) Holman, K. T.; Pivovar, A. M.; Ward, M. D. *Science* **2001**, *294*, 1907. (b) Thalladi, V. R.; Brasselet, S.; Blaser, D.; Boese, R.; Zyss, J.; Nangia, A.; Desiraju, G. R. *Chem. Commun.* **1997**, 1841. (c) Frankenbach, G. M.; Etter, M. C. *Chem. Mater.* **1992**, *4*, 272, 278.

(7) (a) Fernandez-Lopez, S.; Kim, H. S.; Choi, E. C.; Delgado, M.; Granja, J. R.; Khasanov, A.; Kraehenbuehl, K.; Long, G. *Nature* **2001**, *412*, 452. (b) Bong, D. T.; Clark, T. D.; Granja, J. R.; Ghadiri, M. R. *Angew. Chem., Int. Ed.* **2001**, *40*, 988.

(8) (a) Brunet, P.; Simard, M.; Wust, J. D. *J. Am. Chem. Soc.* **1997**, *119*, 2737. (b) Russel, V. A.; Evans, C. C.; Li, W.; Ward, M. D. *Science* **1997**, *276*, 575. (c) Endo, K.; Sawaki, T.; Kobayashi, M.; Masuda, H.; Aoyama, Y. *J. Am. Chem. Soc.* **1995**, *117*, 8341.

(9) (a) Szejtli, J., Osa, T., Eds. *Comprehensive Supramolecular Chemistry*; Pergamon/Elsevier: Oxford, U.K., 1996; Vol. 3 (cyclodextrins). (b) Saenger, W. In *Inclusion Compounds*; Atwood, J. L., Davies, J. E., MacNicol, D. D., Eds.; Academic: New York, 1984; Vol. 2, p 231. (c) Bender, M. L.; Komiyama, M. *Cyclodextrin Chemistry*; Springer-Verlag: New York, 1978; Chapter 3. (d) Szejtli, J. *Chem. Rev.* **1998**, *98*, 1743. (e) Rekharsky, M. V.; Inoue, Y. *Chem. Rev.* **1998**, *98*, 1875. (f) Connors, K. A. *Chem. Rev.* **1997**, *97*, 1325.

(10) Wylie, R. S.; Macartney, D. H. *J. Am. Chem. Soc.* **1992**, *114*, 3136.

(11) (a) Wenz G.; Han, B. H.; Muller, A. *Chem. Rev.* **2006**, *106*, 782. (b) Harada, A.; Li, J.; Kamachi, M. *Nature* **1992**, *356*, 325. (c) Liu, Y.; You, C. C.; Zhang, H. Y.; Kang, S. Z.; Zhu, C. F.; Wang, C. *Nano Lett.* **2001**, *1*, 614. (d) Zhao, T.; Beckham, H. W. *Macromolecules* **2003**, *36*, 9859. (e) Michels, J. J.; O'Connell, M. J.; Taylor, P. N.; Wilson, J. S.; Cacialli, F.; Anderson, H. L. *Chem.—Eur. J.* **2003**, *9*, 6167.

(12) (a) Harada, A.; Li, J.; Kamachi, M. *Nature* **1992**, *364*, 516. (b) Nostro, P. L.; Lopes, J. R.; Cardelli, C. *Langmuir* **2001**, *17*, 4610−4615. (c) Harada, A. *Coord. Chem. Rev.* **1996**, *148*, 115−133. (d) Li, J.; Ni, X.; Zhou, Z.; Leong, K. W. *J. Am. Chem. Soc.* **2003**, *125*, 1788−1795. (e) Becheri, A.; Nostro, P. L.; Ninham, B. W.; Baglioni, P. *J. Phys. Chem. B* **2003**, *107*, 3979−3987. (f) Liu, Y.; Song, Y.; Wang, H.; Zhang, H. Y.; Li, X. Q. *Macromolecules* **2004**, *37*, 6370. (g) Choi, H. S.; Ooya, T.; Lee, S. C.; Sasaki, S.; Kurisawa, M.; Uyama, H.; Yui, N. *Macromolecules* **2004**, *37*, 6705.

(13) Agbaria, R. A.; Gill, D. *J. Phys. Chem.* **1988**, *92*, 1052.

(14) (a) Agbaria, R. A.; Gill, D. *J. Photochem. Photobiol., A* **1994**, *78*, 161. (b) Zhang, C.; Shen, X.; Gao, H. *Chem. Phys. Lett.* **2002**, *363*, 515.

(15) (a) Li, G.; McGown, L. B. *Science* **1994**, *246*, 249. (b) Pistolis, G.; Malliaris A. *J. Phys. Chem.* **1996**, *100*, 15562.

(16) Pistolis, G.; Malliaris, A. *J. Phys. Chem. B* **1998**, *102*, 1095.

(17) Lee, L. A.; Robb, R. A. *IEEE J. Quantum Electron.* **1980**, *16*, 777.

(18) (a) Lackowicz, J. R. *Principles of Fluorescence Spectroscopy*, 2nd ed.; Plenum Press: New York, 1999. (b) Soper, S. A.; Warner, I. M.; McGown, L. B. *Anal. Chem.* **1998**, *70*, 477.

(19) Pistolis, G.; Malliaris, A. *Langmuir* **1997**, *13*, 1457.

(20) Nijegorodov, N. I.; Downey, W. S. *J. Phys. Chem B* **1994**, *98*, 5639.

(21) Soutar, I.; Swanson, L.; Imhof, R. E.; Rumbles, G. *Macromolecules* **1992**, *25*, 4399.

(22) (a) Perrin, P. F. *J. Phys. Radium* **1934**, *5*, 497. (b) Fleming, G. R. *Chemical Applications of Ultrafast Spectroscopy*; Oxford University Press: London, 1986.

(23) Balabai, N.; Linton, B.; Napper, A.; Priyadarshy, S.; Sukharevsky, A. P.; Waldeck, D. H. *J. Phys. Chem. B* **1998**, *102*, 9617.
(24) Benzler, J.; Luther, K. *Chem. Phys. Lett.* **1997**, *279*, 333.
(25) Singh, M. K.; Pal, H.; Koti, A. S. R.; Sapre, A. V. *J. Phys. Chem. A* **2004**, *108*, 1465.
(26) Tormo, L.; Organero, J. A.; Douhal, A. *J. Phys. Chem. B* **2005**, *109*, 17848.
(27) Sen, P.; Roy, D.; Mondal, S. K.; Sahu, K.; Ghosh, S.; Bhattacharyya, K. *J. Phys. Chem. A* **2005**, *109*, 9716.
(28) Roy, D.; Mondal, S. K.; Sahu, K.; Ghosh, S.; Sen, P.; Bhattacharyya, K. *J. Phys. Chem. A* **2005**, *109*, 7359.
(29) Godik, V. A.; Sablygin, M. Y.; Rodionov, A. N.; Simonov, A. P.; Shigorin, D. N. *Russ. J. Phys. Chem.* **1985**, *59*, 374, 377.
(30) Troxler, T.; Smith, P. G.; Topp, M. R. *Chem. Phys. Lett.* **1993**, *211*, 371.
(31) Roi, M.; Doraiswamy, S. *J. Chem. Phys.* **1993**, *98*, 3213.
(32) Zhao, Y. H.; Abraham, M. H.; Zissimos, A. M. *J. Org. Chem.* **2003**, *68*, 7368.
(33) Schiller, R. L.; Lincoln, S. F.; Coates, J. H. *J. Chem. Soc., Faraday Trans.* **1987**, *83*, 3227.
(34) Park, H. R.; Mayer, B.; Wolschann, P.; Kohler, G. *J. Phys. Chem.* **1994**, *98*, 6158.
(35) Cox, G. S.; Hauptman, P. J.; Turro, N. *J. Photochem. Photobiol.* **1984**, *39*, 597.
(36) (a) Pistolis, G.; Malliaris, A. *Chem. Phys. Lett*. **1999**, *303*, 334. (b) *Chem. Phys. Lett*. **1999**, *310*, 501.
(37) Behr, J. P.; Lehn, J. M. *J. Am. Chem. Soc.* **1976**, *98*, 1743.
(38) Maus, M.; Mitra, S.; Lor, M.; Hofkens, J.; Weil, T.; Herrmann, A.; Mullen, K.; De Schryver, F. C. *J. Phys. Chem. A* **2001**, *105*, 3961.
(39) Steiner, T.; Gessler, K.; Saenger, W. *Carbohydr. Res.* **1994**, *260*, 27.
(40) Organero, J. A.; Douhal A. *Chem. Phys. Lett.* **2003**, *373*, 426.
(41) Pistolis, G. *Chem. Phys. Lett*. **1999**, *304*, 371.
(42) (a) Bohne, C.; Konuk, R.; Scaiano J. C. *Chem. Phys. Lett*. **1988**, *152*, 15. (b) Yamazaki, I.; Winnik, F. M.; Winnik M. A.; Tazuke S. *J. Phys Chem*. **1987**, *91*, 4213.
(43) (a) Silva, A. P.; Gunarathe, H. Q. N.; Gunnlaugsson, T.; Huxley A. J. M.; McCoy, C. P.; Rademacher, J. T.; Rice T. E. *Chem. Rev.* **1997**, *97*, 1515. (b) Tsujii, Y.; Itoh, T.; Fukuda, T.; Miyamoto, T.; Ito, S.; Yamamoto, M. *Langmuir* **1992**, *8*, 936.
(44) (a) Mizuno, K.; Matsui, A. *J. Lumin.* **1987**, *38*, 323. (b) Sumi, H. *Chem. Phys.* **1989**, *130*, 433.
(45) (a) Horrocks, D. L. *J. Chem. Phys*. **1967**, *47*, 3089. (b) Lami, H.; Laustriat, G. *J. Chem. Phys.* **1968**, *48*, 1832.
(46) Roberts, A. J.; Cureton, C. G.; Phillips, D. *Chem. Phys. Lett*. **1980**, *72*, 554.
(47) (a) Pistolis, G.; Malliaris, A. *Supramol. Chem*. **2003**, *15*, 395. (b) Pistolis, G.; Malliaris, A. *J. Phys. Chem. B* **2004**, *108* (9), 2846.
(48) (a) Kano, K.; Takenoshita, I.; Ogawa, T. *Chem. Lett.* **1982**, 321. (b) Hamai, S. *J. Phys. Chem*. **1989**, *93*, 6527. (c) Herkstroeter, W. G.; Martic, P. A.; Farid, S. *J. Chem. Soc., Perkin Trans. 2* **1984**, 1453. (d) De Feyter, S.; Stam, J. V.; Imans, F.; Viaene, L.; De Schryver, F. C.; Evans, C. H. *Chem. Phys. Lett*. **1997**, *277*, 44. (e) Raj, C. R.; Ramaraj, R. *Chem. Phys. Lett*. **1997**, *273*, 285. (f) Agbaria, R. A.; Roberts, E.; Warner, I. M. *J. Phys. Chem*. **1995**, *99*, 10056.
(49) Eric W. Weisstein. "Spheroid". From *MathWorld*—A Wolfram Web Resource. http://mathworld.wolfram.com/Spheroid.html.